Simultaneous Measurement of Strain and Temperature Using Two-Mode Elliptical Core Optical Fiber

By

Zhi G. Wang

Thesis submitted to the Faculty of the
Virginia Polytechnic Institute and State University
in partial fulfillment of the requirements for the degree of
Masters of Science

in

Electrical Engineering

APPROVED:

Richard O. Claus

Dr. Richard O. Claus, Chairman

Dr. Ioannis M. Besieris

Dr. Ting C. Poon

June, 1992
Blacksburg, Virginia

Simultaneous Measurement of Strain and Temperature Using Two-Mode Elliptical Core Optical Fiber

by

Zhi G. Wang

Richard O. Claus, Chairman

Electrical Engineering

(ABSTRACT)

A single piece of optical fiber can be utilized to sense both strain and temperature simultaneously. To develop such a sensor, we sandwich a section of two-mode elliptical core (e-core) fiber between two partially reflecting mirrors. This configuration can be considered as an intrinsic Fabry-Perot interferometer, in which the two-mode, e-core fiber serves as the resonant cavity. Two different types of phase modulation can be extracted under perturbations of strain and temperature on the fiber. These phase changes are due to the two-mode interference and intrinsic Fabry-Perot interference, respectively. The relationship between the phase information and the two physical measurands, i.e. strain and temperature, can be established using two coupled equations, in which the strain and temperature are considered as two unknowns. By solving these two coupled equations, we can simultaneously determine the strain and temperature. The waveguide theory and the cross sensitivity analysis of this sensor are presented. The descriptions of four independent experiments that have been used to determine the coefficients of the two coupled equations are given. The resolutions of the strain and temperature measurements have been obtained to be 31 μm/m and 4.5 °C, respectively.

Acknowledgements

I would like to express my sincere gratitude to Dr. Richard O. Claus for his inspiration and support in the development of this research project and for serving as my academic advisor during the past two years. I would like to thank Dr. Ioannis M. Besieris and Dr. Ting C. Poon for serving as my graduate committee members. My acknowledgements extend to Dr. Ashish M. Vengsarkar and Mr. Kent A. Murphy for introducing their original idea of this research topic to me and for their technical advice and support on this project. I should thank Dr. Anbo Wang for generously giving his time and effort in helping me to understand fiber optic sensing technology. I would also like to acknowledge all other faculty, staff members, and students in Fiber & Electro-Optics Research Center (FEORC) for their support in numerous ways in the past two years.

My acknowledgment also goes to those who taught me physics, from which I have benefited immensely during my study here in Virginia Tech. They are Dr. C.Y. Yang, Dr. K.H. Liu, Dr. W.E. Collins and Dr. D. Bagayoko in Southern University, Baton Rouge, Louisiana, and Dr. M.S. Conradi, Dr. A.E. Carlsson and Dr. J. Klarmann in Washington University, St. Louis, Missouri.

On my family side, it would be too little just to say "thanks" to my great grand father, S.G. Chow, without whom I would never have any chance to come to the States for higher education. He died of a heart attack two years ago in Baton Rouge, Louisiana. His kindness, generosity and humor always live in my heart. I would like to acknowledge my other relatives in Baton Rouge, Louisiana, including my great grand mother, Y.F. Shih Chow, and her daughters (my great aunts), B.L. Chow Lam, B.C. Chow Hu, and B.C. Chow Chen, for their financial and moral support during my higher education here in the States. Finally, I would like to acknowledge my parents, H.S. and M.Q. Wang, and my two sisters, H.M. Wang and Y.Z. Wang, for their love and care. Every letter or phone call from my home in China has always comforted me as well as animated me. We have always shared both the hardship and joy together.

This research was sponsored in part by CIT (Center for Innovative Technology, Virginia) and by donations of the faculty and staff members in FEORC.

Contents

1. Introduction

1.1 Definition of fiber optic sensor

Technically, a sensor or measurement transducer is a device that converts the state of a particular physical measurand into an easily readable form. For example, a simple thermometer effectively converts temperature into a number indicating the height of mercury. Sensors are present in every walk of our modern life. A smoke alarm in a kitchen, a speedometer in a car, and a guidance detector in a rocket are all sensors. Optical fibers have long been recognized as transmission media in the optical communication industry. Because of the fact that optical fibers have also many other useful characteristics, they have been widely utilized in sensing technology. A sensor that is constructed based upon the physical principles of optical fiber can be generally referred to as a fiber optic sensor.

1.2 Types of sensors

It has been demonstrated that optical fibers can be employed to sense temperature, pressure, strain, magnetic fields, and other physical parameters. All fiber optic sensors can be classified into two types. They are intensity-modulated and phase-modulated sensors. To clarify this concept, let us express the electrical field inside an optical fiber in the simplified form, viz.

$$E = A \sin (kx - \omega t + \psi), \tag{1.1}$$

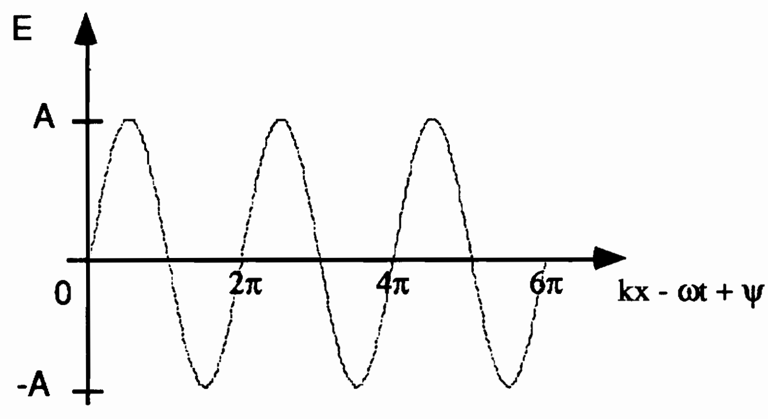

Figure 1-1. A typical electrical field E versus its phase kx - ωt + ψ

where A is the amplitude, k is the wave number, ω is the angular frequency and ψ is the initial phase of the electric field. These four parameters are constants for a given field. A plot of electric field versus the phase is shown in Figure 1-1. The intensity of this wave is defined as

$$I = \langle E^2 \rangle = A^2 / 2, \tag{1.2}$$

where $\langle\, \rangle$ represents the time average over a complete cycle of the electrical field. A plot of this intensity versus phase is shown in Figure 1-2.

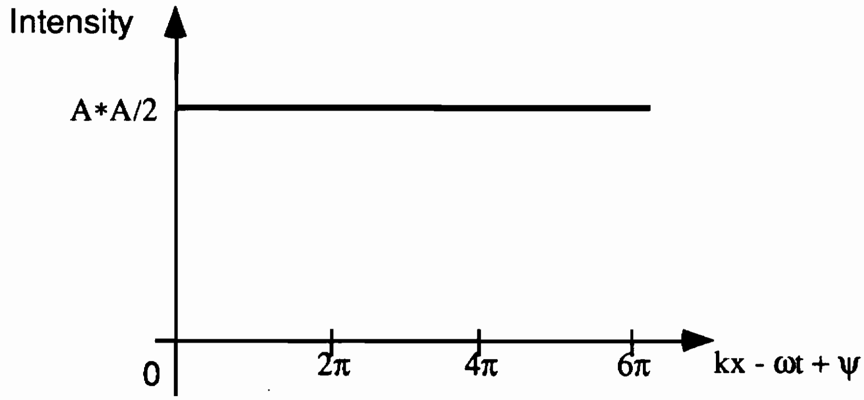

Figure 1-2. The corresponding intensity of the electrical field versus the phase.

The operation of intensity-modulated optical fiber sensors is based upon the fact that optical intensity may be made to change due to changing environments, such as temperature, displacement, speed of rotation and other factors. In most applications, wide band light sources, such as LEDs and white light sources, are used. Multimode fibers are ideal for most intensity-modulated sensors. Geometric optics is often applied to describe intensity-based sensor behaviors.

Phase-modulated fiber optic sensors, on the other hand, operate based upon the change of phase term, $kx - \omega t + \psi$, due to the changing environment. This type of sensor is also known as an interferometric sensor. Mach-Zehnder, Michelson, Sagnac and Fabry-Perot fiber interferometers are examples of phase-modulated fiber sensors. The names of these sensors are derived from those of their bulk optic counterparts. Because the simultaneous measurement of strain and temperature using two-mode elliptical core (e-core) optical fiber is an application of phase modulated sensors, interferometric sensors require further exploration here. In the next section, a simple Mach-Zehnder fiber interferometer is studied as an example in order to demonstrate the operation of a typical phase-modulated sensor system.

1.3 Mach-Zehnder fiber interferometer

The schematic diagram of a Mach-Zehnder fiber interferometer is shown in Figure 1-3.

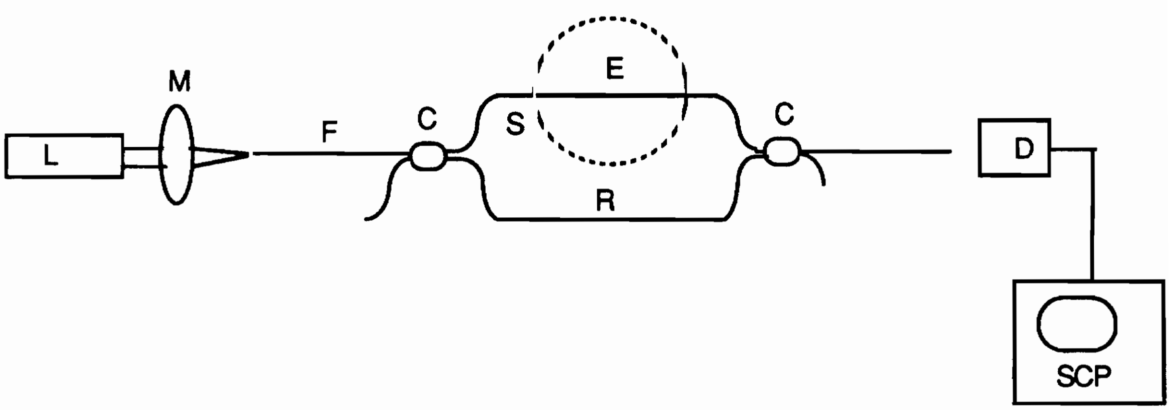

Figure 1-3. Mach-Zehnder fiber interferometer.

L: Laser (wavelength λ); M: Microscope objective;F: Single mode fiber at λ; C: 2x2 single mode coupler at λ; S: Sensing fiber arm; R: reference fiber arm; E: Environment to be monitored; D: Photodetector; SCP: Oscilloscope.

Here, a collimated laser beam of wavelength λ is focused into a single mode fiber through a microscope objective. Since this fiber supports only one mode at the wavelength λ, the electric field inside the fiber can be treated nearly as a plane wave. At the 2x2 coupler, the optical power is divided into reference and sensing arms. The sensing arm experiences a changing environment such as changes in temperature, axial strain, pressure and magnetic fields, which will generally affect the length of the sensing fiber arm or the polarization state of the light or other effects [1]. The light traveling in the reference arm does not experience this modulation. The two optical signals are combined and divided into two paths at the output of the second 2x2 coupler. One of these output fibers is fed to the photodetector where the intensity is detected. The other output fiber is generally disregarded. The intensity information is converted into an electrical signal (voltage) which is carried on to an amplifier. The amplified signal is finally shown on the oscilloscope. It must be emphasized that the output optical signal is the result of interference between the light in the sensing and reference arms because these two light beams are generated from the same source (the laser). It is also important that the difference between the sensing fiber length and the reference fiber length must be less than the coherence length of the light source [2].

Figure 1-4 further clarifies the action of interference in a Mach-Zehnder sensing system.

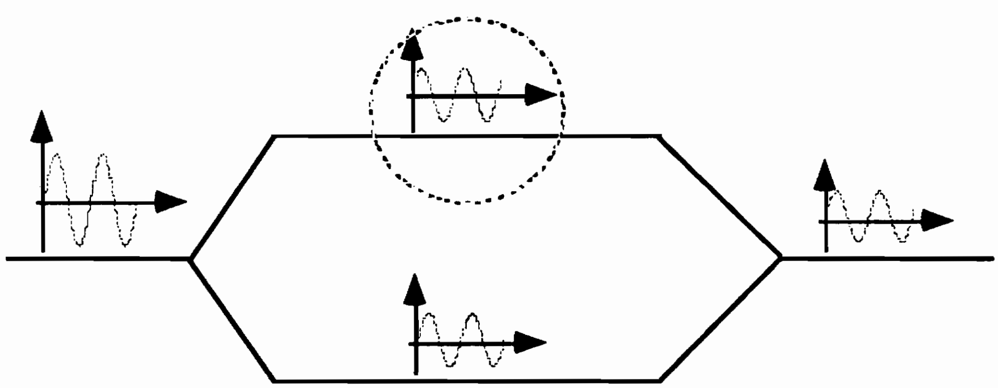

Figure 1-4 (a). Electric field pattern in Mach-Zehnder interferometer.

Mathematically, the interference can be described by the following.

The electric field in the input fiber:

$$E = A \sin (kx - \omega t). \tag{1.3}$$

The electric field in reference arm:

$$E_r = \frac{A}{\sqrt{2}} \sin (kx - \omega t). \tag{1.4}$$

The electric field in sensing arm:

$$E_s = \frac{A}{\sqrt{2}} \sin (kx - \omega t + \Delta\phi), \tag{1.5}$$

where $\Delta\phi$ is the phase change induced by the external environment. We ignore the initial phase difference between the reference and sensing arms and also assume the couplers have a 50-50 power splitting ratio.

The total field in one of the outputs:

$$E_t = \frac{1}{\sqrt{2}}(E_r + E_s). \tag{1.6}$$

The intensity of the reference arm:

$$I_r = < E_r^2 > = A^2/2. \tag{1.7}$$

The intensity of the sensing arm:

$$I_s = < E_s^2 > = A^2/2. \tag{1.8}$$

The intensity of the output fiber:

$$\begin{aligned} I_t &= < E_t^2 > \\ &= 1/2\,(I_r + I_s + 2\,A^2 < \sin(kx - \omega t)\sin(kx - \omega t + \Delta\phi) >) \\ &= A^2 \cos^2(\Delta\phi/2). \end{aligned} \tag{1.9}$$

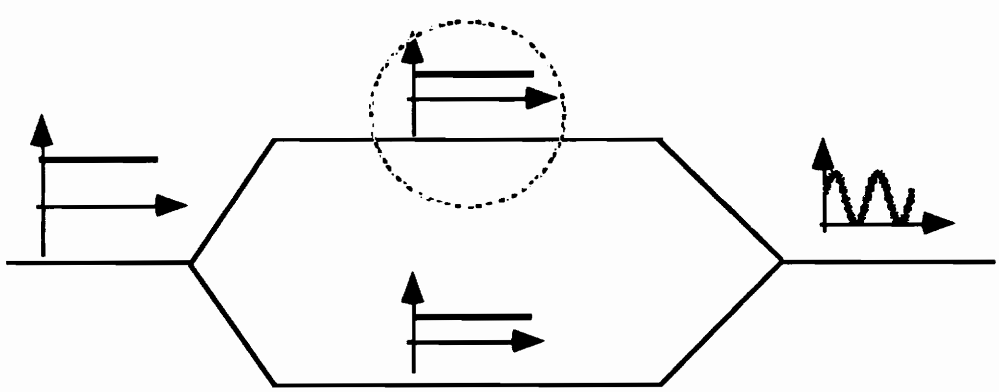

Figure 1-4 (b). Optical intensity levels in Mach-Zehnder interferometer.

In reality, $\Delta\phi$ very often represents the phase difference between the fields in the reference and sensing fibers induced by the elongation of the sensing fiber. Therefore,

$$\Delta\phi = 2\pi\,\Delta L/\lambda, \tag{1.10}$$

and the intensity expression at the output becomes

$$I_t = A^2 \cos^2(\pi\,\Delta L/\lambda), \tag{1.11}$$

where λ is the wavelength of light source and ΔL is the change of fiber length, which may be caused by temperature, strain, pressure and other parameters. The output of a typical interferometric sensor is shown in Figure 1-5.

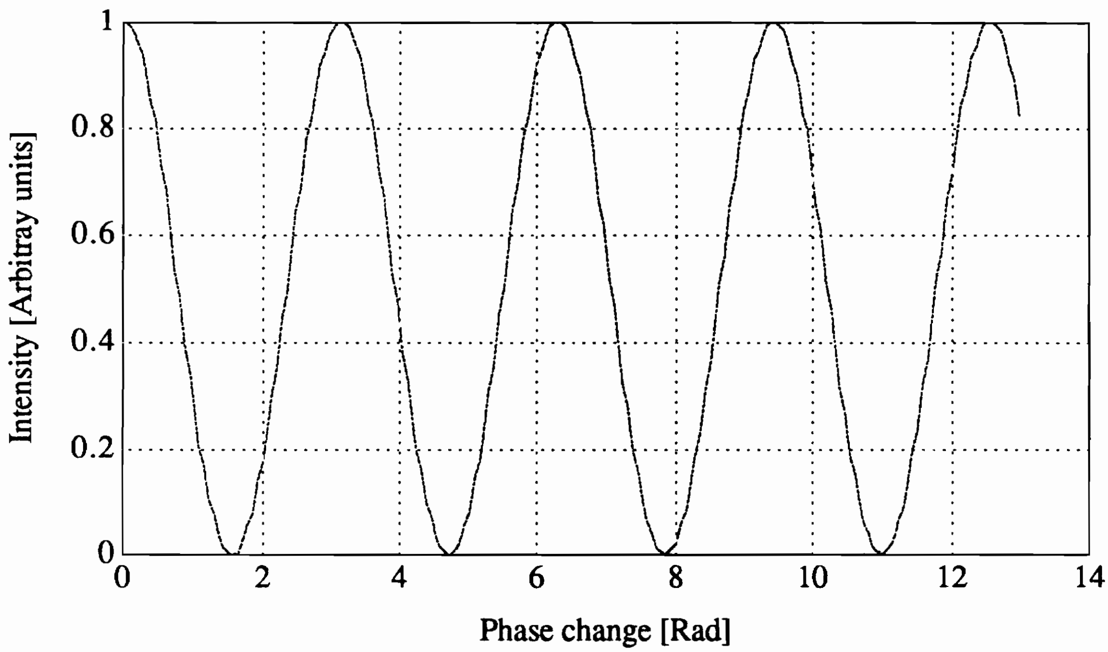

Figure 1-5. Typical interference fringes.

By counting the number of sine wave periods (fringes), we can determine the phase induced, $\Delta\phi$, from which the exact value of the environmental measurand monitored can be derived. It must be noted that the fringe signal only appears when the environmental perturbation is active. In other words, if the measurands are stable, there will be a flat DC line (constant) on the oscilloscope. Such an effect can also be seen by setting ΔL equal to a constant, which results in a constant intensity output (I_t) in Eq.(1.11).

1.4 Advantages of optical fiber sensors

In general, optical fiber transducers require much more complicated signal processing systems and supporting components than their electronic counterparts. They are also more difficult to fabricate and thus they often cost more than conventional electronic sensors.

However, optical fiber sensors posses many unique features that electronic sensors cannot match. They are:

(1) High sensitivity. Changes of optical phase can be detected very precisely.
(2) Light weight. Dielectric materials weigh less than metals. This is crucial in the aerospace and many other industries.
(3) Environmental ruggedness. Optical fiber is immune to electromagnetic interference and may be ruggedized to vibration and shock.
(4) High temperature performance. The melting point of quartz glass is about 1400°C. Optical fiber can be used to sense temperature and other physical parameters such as strain and pressure in a high temperature environment.

The rest of the thesis is divided as follows. Chapter 2 describes a simultaneous measurement scheme using two-mode, e-core fibers. In Chapter 3, starting with Maxwell's equations, general field expressions of both the LP_{01} and LP_{11}^{even} modes are derived, and the field expressions of the two-lobe interferometer and intrinsic Fabry-Perot interferometer combined are obtained. The cross sensitivity issue is analyzed in Chapter 4. Chapter 5 contains the four independent experiments performed to seek four sensitivity coefficients. Detailed experimental procedures and considerations about many practical problems are also discussed. The resolution of this sensor is addressed in Chapter 6. Conclusions of this research and comments about potential applications are presented in Chapter 7.

2. Simultaneous measurement of physical measurands

2.1 Definition of simultaneous measurement

A single piece of fiber can be utilized to sense more than one physical measurand, such as strain and temperature, at the same time. This sensing technique is referred to as simultaneous measurement or multiple parameter measurement.

2.2 Importance of simultaneous measurement

There are two major motivations for simultaneous measurement. The first motivation is an economic consideration. Optical fiber sensors may be constructed as a network over a large area of material to monitor the health of the material and structure. This configuration is known as a "smart structure" and has direct applications in the aerospace industry. Very often the fiber network is embedded inside the material to potentially provide complete lifetime monitoring. It is natural to use these embedded fibers to extract as much information as possible, for it will be too expensive to use different fibers to monitor different environmental parameters. Thus the simultaneous measurement of several parameters is required. The second motivation for simultaneous measurement is that to measure one parameter such as strain, a signal resulting from another parameter, for example temperature, is also inevitably introduced. In other words, it is difficult to make a measurement specific. Many temperature-compensated strain gauge optical fiber sensors have been proposed [3,4,5,6]. One successful temperature-insensitive strain sensor was invented by Murphy *et al.* [7] and practically employed to measure strain in a high temperature facility at the NASA-Langey Research Center. One alternative solution for separating strain and temperature is to simultaneously measure both.

Strain and temperature are the most frequently encountered physical parameters in the environment of our interest. What we would like to measure are change of temperature (ΔT) with respect to an initial state and strain, which can be defined as

$$\Delta\varepsilon = \Delta L / L, \tag{2.1}$$

where ΔL is the fiber elongation and L is the total length of the fiber.

2.3 Using two-mode elliptical core fiber

To simultaneously measure two physical quantities using a single piece of fiber, two different physical configurations within the fiber are required such that each of the two parameters can be uniquely determined.

A two-mode, e-core fiber has been demonstrated to be effective for the sensing of strain and temperature. It has also been shown that it can be used to construct many optical fiber components such as frequency shifters [8], modal couplers [9], and optical switches [10]. Since the fiber is operated in its two-mode regime, only the LP_{01} and LP_{11}^{even} modes are excited inside the fiber (the detailed waveguide theory is presented in Chapter 3). These two linearly polarized modes interfere and produce a two-lobe spatial intensity distribution in the fiber. Figure 2-1 shows this phenomenon.

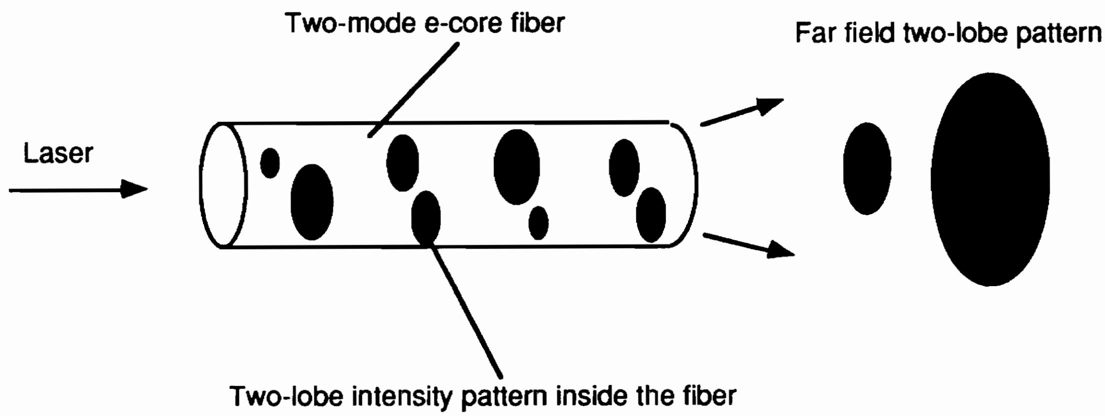

Figure 2-1.Two-lobe intensity pattern

Since the e-core fiber is highly birefringent, the two-lobe intensity pattern is stable [11]. It is also realized that the spatial distribution of the intensity outside the fiber endface (i.e. in the far field) retains the two-lobe intensity pattern with a $\pi/2$ phase shift relative to the pattern at the fiber endface due to diffraction effects [12]. The shape of the two-lobe intensity pattern can be modulated by both axial strain and temperature. The two-lobe interferometer alone is able to sense either strain or temperature but not both at the same time. To simultaneously determine strain and temperature, one more physical configuration must be incorporated into this two-mode, e-core fiber. Huang [13], Vengsarkar [14], and

Wang [15] have demonstrated different schemes of simultaneous measurement using two-mode, e-core fibers. However, all of these schemes either require complicated signal processing systems or are otherwise cumbersome, which realistically make them less attractive for smart structure and embedding applications.

2.4 Fabry-Perot configuration

To effectively reduce the size and weight of the sensing system while keeping the signal processing system as simple as possible, a novel simultaneous measurement device is proposed, in which an intrinsic Fabry-Perot interferometer (IFPI) is incorporated into the two-mode, e-core fiber to resolve strain and temperature. The schematic diagram of this configuration is shown in Figure 2-2.

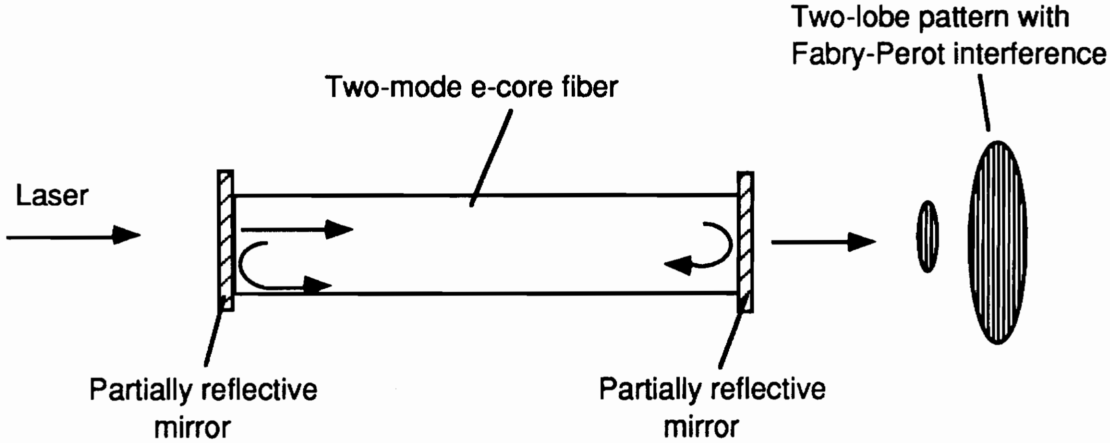

Figure 2-2. Two-lobe intensity pattern with IFPI.

The fiber section between the two partially reflective mirrors serves as a Fabry-Perot cavity. The interference signal of the Fabry-Perot interferometer is encoded within the two-lobe intensity pattern at the far field. A spatial filter with a photodetector at the far field can pick up both the two-mode and Fabry-Perot interference signals. Notice further that the far field two-lobe pattern with Fabry-Perot interference fringes in Figure 2-2 appears only in the presence of continuous perturbation on the fiber. If the environment is stable, there will be just the two-lobe pattern instead of Fabry-Perot interference signal modulated by the two-lobe intensity pattern.

2.5 Demodulation technique

Theoretically, the two-mode interference signal, Fabry-Perot interference signal and the superposition of both can be plotted as shown in Figure 2-3.

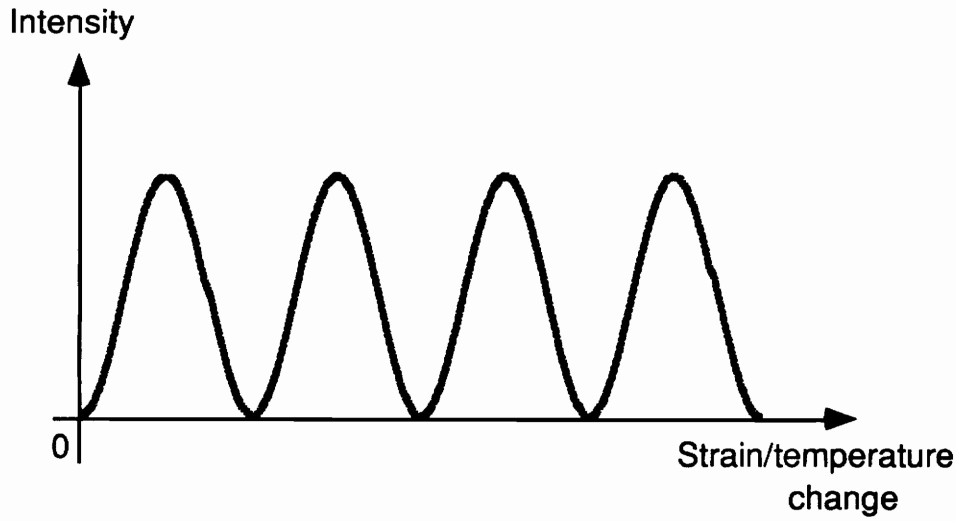

Figure 2-3 (a) Two-mode interference signal.

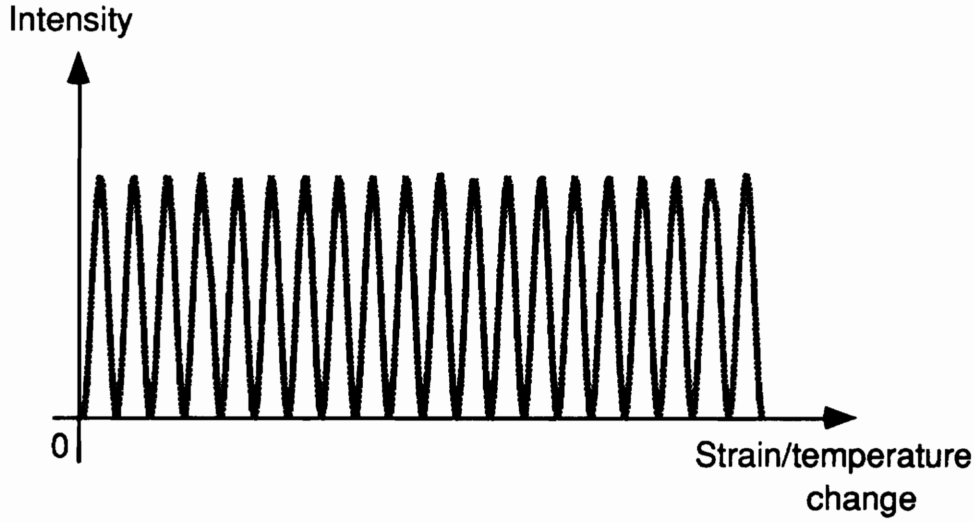

Figure 2-3 (b) Intrinsic Fabry-Perot interference signal.

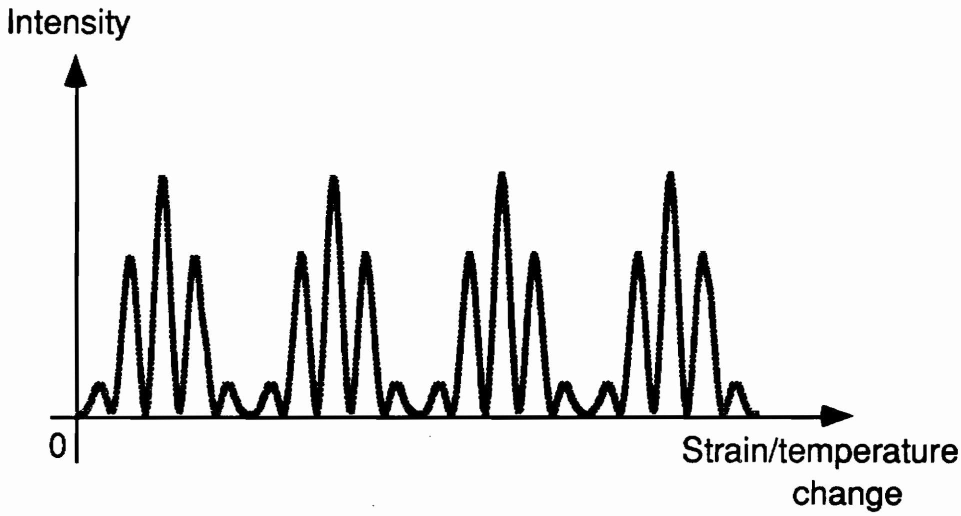

Figure 2-3 (c) The superposition of both the two-mode and Fabry-Perot interferometer signals

From Figure 2-3 (c), we can derive two phases, $\Delta\theta_1$ and $\Delta\theta_2$, which correspond to the Fabry-Perot and the two-lobe signals, respectively. In reality, both $\Delta\theta_1$ and $\Delta\theta_2$ depend on strain and temperature in the fiber to different extents. Two coupled equations containing both strain ($\Delta\varepsilon$) and temperature change (ΔT) can be established. For a first order approximation (the detailed analysis is presented in Chapter 4), these conditions can be expressed by

$$\Delta\theta_1 = A * \Delta\varepsilon + B * \Delta T, \tag{2.2a}$$

and

$$\Delta\theta_2 = C * \Delta\varepsilon + D * \Delta T, \tag{2.2b}$$

where A, B, C, and D are constants that can be determined experimentally through calibration procedures. By counting both Fabry-Perot and the two-lobe fringes using this configuration, we can determine both $\Delta\theta_1$ and $\Delta\theta_2$, and use Eqs.(2.2a) and (2.2b) to simultaneously resolve the strain ($\Delta\varepsilon$) and temperature (ΔT) on the fiber.

3. Waveguide theory

The two-lobe spatial intensity distribution inside a two-mode, e-core fiber is the result of the interference between the LP_{01} and LP_{11}^{even} linearly polarized modes. To thoroughly understand this phenomenon, the electric field expression inside the fiber must be derived. Then the square of this electric field can be expressed to describe the spatial intensity distribution on a cross section of the fiber core. To accomplish this task, Maxwell's equations are employed along with appropriate boundary conditions for a cylindrical dielectric wave guide. The effect of Fabry-Perot interference can also be incorporated with the two-lobe pattern in terms of derived electric fields.

3.1 Setting up the wave equation using Maxwell's equations

To find the electric field in the fiber, we use the cylindrical coordinate system as shown in Figure 3-1.

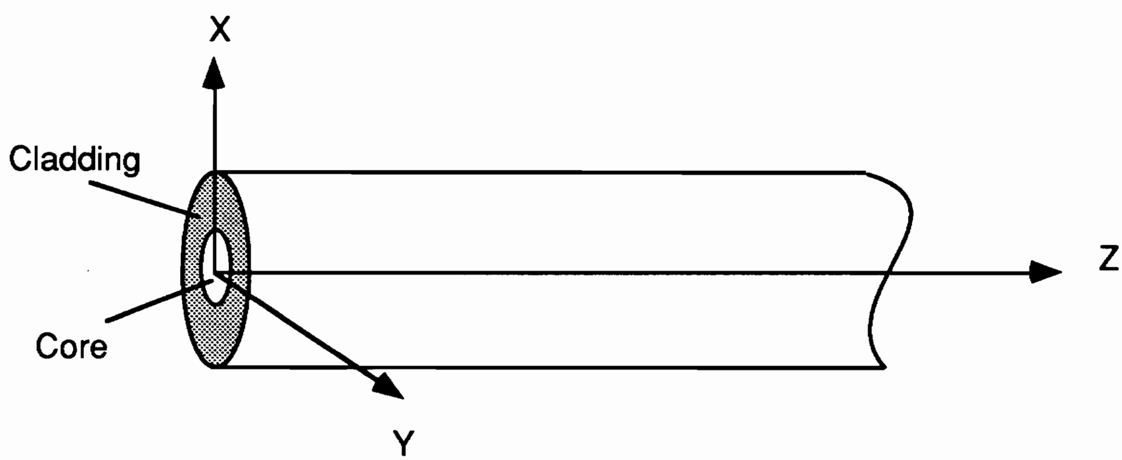

Figure 3-1 (a). Cylindrical coordinate system.

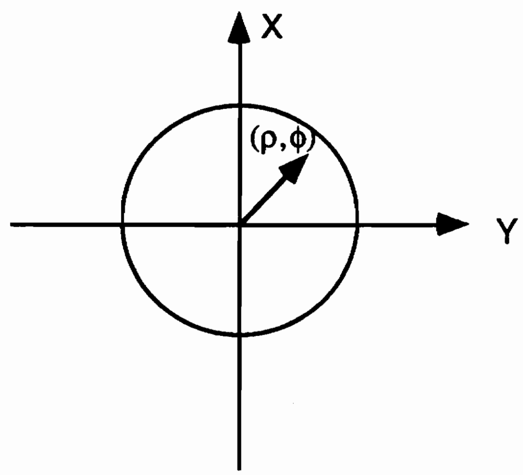

Figure 3-1(b). Cross section of the fiber core.

We will use a circular waveguide instead of an elliptical waveguide in analyzing the two-mode, e-core fiber. To obtain the electric field at a point (ρ,ϕ,z) inside the fiber core, we apply Maxwell's equations for a source-free and lossless dielectric (glass) medium, viz.

$$\nabla x\vec{E} = -j\,\omega\mu\vec{H}, \text{ and} \tag{3.0a}$$

$$\nabla x\vec{H} = j\,\omega\varepsilon\vec{E}, \tag{3.0b}$$

where $\vec{E}$ and $\vec{H}$ are the electric and magnetic fields at (ρ,ϕ,z) in the fiber core, respectively, and ω is the angular frequency of the light source. In this cylindrical coordinate system, a guided wave which propagates in the fiber along the positive z axis can be expressed as

$$\vec{E} = \mathrm{Re}\left\{\vec{E_0}(\rho,\phi)\exp\left[j(\omega t - \beta_g z)\right]\right\}, \tag{3.1a}$$

$$\vec{H} = \mathrm{Re}\left\{\vec{H_0}(\rho,\phi)\exp\left[j(\omega t - \beta_g z)\right]\right\}, \tag{3.1b}$$

where β_g is the phase constant of the wave. Using Eqs. (3.0a) and (3.0b), $\vec{E_o}$ and $\vec{H_o}$ can be expressed in terms of their field components (scalars) as

$$E_\rho = -\frac{j}{\beta_c^{\,2}}\left(\beta_g\frac{\partial E_z}{\partial \rho} + \omega\mu\frac{1}{\rho}\frac{\partial H_z}{\partial \phi}\right), \tag{3.2a}$$

$$E_\phi = -\frac{j}{\beta_c^2}\left(\beta_g \frac{1}{\rho}\frac{\partial E_z}{\partial \phi} - \omega\mu \frac{\partial H_z}{\partial \rho}\right), \tag{3.2b}$$

$$H_\rho = -\frac{j}{\beta_c^2}\left(\beta_g \frac{\partial E_z}{\partial \rho} - \omega\mu \frac{1}{\rho}\frac{\partial H_z}{\partial \phi}\right), \tag{3.2c}$$

$$H_\phi = -\frac{j}{\beta_c^2}\left(\beta_g \frac{1}{\rho}\frac{\partial E_z}{\partial \phi} + \omega\mu \frac{\partial H_z}{\partial \rho}\right), \tag{3.2d}$$

$$\frac{\partial^2 E_z}{\partial \rho^2} + \frac{1}{\rho}\frac{\partial E_z}{\partial \rho} + \frac{1}{\rho^2}\frac{\partial^2 E_z}{\partial \phi^2} + \beta_c^2 E_z = 0 \text{ , and} \tag{3.3a}$$

$$\frac{\partial^2 H_z}{\partial \rho^2} + \frac{1}{\rho}\frac{\partial H_z}{\partial \rho} + \frac{1}{\rho^2}\frac{\partial^2 H_z}{\partial \phi^2} + \beta_c^2 H_z = 0 , \tag{3.3b}$$

where

$$\beta_c^2 = \beta^2 - \beta_g^2 \text{ and } \beta^2 = \omega^2\mu\varepsilon . \tag{3.4}$$

In order to determine the electric and magnetic fields, and hence the intensity inside the fiber, we must solve the two differential equations (3.3a) and (3.3b) with appropriate boundary conditions and then substitute E_z and H_z into Eqs. (3.2a) through (3.2d) to obtain the other field components.

3.2 The concept of a propagation mode

There is a problem solving Eqs. (3.3a) and (3.3b) because, as indicated in Eq. (3.4), β_c is an unknown (for β_g is an unknown). The phase constant β_g can be determined by imposing the field boundary conditions at the interface between the core and the cladding. It turns out (it will be shown) that there are many β_g that satisfy the same boundary conditions. We will also show that there are many such waves with different β_g which can propagate in the fiber. Each of these waves is referred to as a wave mode. Different wave modes have different phase velocities. In fiber optic communication, single mode operation is often preferred in order to avoid intermodal dispersion of signals. The rest of this section is used to determine β_g and the number of guided modes for a given structure (fiber configuration) and light source frequency (ω).

Starting with Eq.(3.3a) (a similar procedure can be used for Eq.(3.3b)), we apply the method of separation of variables. Assume that

$$E_z = P(\rho)\ \Phi(\phi)\ . \tag{3.5}$$

Substitute into Eq.(3.3a), to obtain

$$\frac{\partial^2 \Phi}{\partial \phi^2} + n^2\ \Phi = 0\ \text{, and} \tag{3.6}$$

$$\frac{\partial^2 P}{\partial \rho^2} + \frac{1}{\rho}\frac{\partial P}{\partial \rho} + \left(\beta_c^2 - \frac{n^2}{\rho^2}\right) P = 0\ , \tag{3.7}$$

where n is an integer. The solution of Eq.(3.6) may be expressed as a sine (or cosine) wave and the solution of Eq.(3.7) in terms of Bessel functions of order n. For a given structure, let n_1 and n_2 be the refractive indices of the fiber core and cladding, respectively. In order to satisfy the total internal reflection condition, we demand

$$n_1 > n_2 . \tag{3.8}$$

We further require that the electric field in the core be finite and the electric field in the cladding decay radially outward. Therefore, a general solution can be written as

$$E_z = \left(A_1 J_n(\beta_c \rho) + B_1 K_n(|\beta_c| \rho)\right)\left(C_1 \sin(n\phi) + D_1 \cos(n\phi)\right), \tag{3.9}$$

where A_1, B_1, C_1 and D_1 are all constants. Since β_c is real in the core region and imaginary in the cladding region, consulting Eq.(3.4), we obtain

$$k\, n_2 < \beta_g < k\, n_1 \tag{3.10}$$

where k is the propagation constant of a plane wave in free space. For the sake of discussion,we define

$$u = \left(k^2 n_1^2 - \beta_g^2\right)^{1/2} a \text{, and} \tag{3.11a}$$

$$w = \left(\beta_g^2 - k^2 n_2^2\right)^{1/2} a \text{,} \tag{3.11b}$$

where "a" is the radius of the fiber core. Combining Eqs. (3.11a) and (3.11b), we obtain

$$u^2 + w^2 = k^2 n_1^2 a^2 \Delta \text{, and} \tag{3.12a}$$

$$\Delta = \frac{n_1^2 - n_2^2}{2 n_1^2} \text{.} \tag{3.12b}$$

Keep in mind that u and w contain the phase constant β_g. Substituting Eq.(3.9) into Eqs. (3.2a) through (3.2d), and similarly after solving Eq.(3.3b) and substituting H_z into Eqs.(3.2a) through (3.2d), the rest of field components can be found.

To determine β_g and the propagation mode characteristics, we impose the following boundary conditions, namely,

$$E_z^{core}(\rho = a) = E_z^{cladding}(\rho = a), \tag{3.13a}$$

$$E_\phi^{core}(\rho = a) = E_\phi^{cladding}(\rho = a), \tag{3.13b}$$

$$H_z^{core}(\rho = a) = H_z^{cladding}(\rho = a), \tag{3.13c}$$

$$H_\phi^{core}(\rho = a) = H_\phi^{cladding}(\rho = a), \tag{3.13d}$$

$$H_\rho^{core}(\rho = a) = H_\rho^{cladding}(\rho = a) \text{, and} \tag{3.13e}$$

$$\varepsilon_1 E_\rho^{core}(\rho = a) = \varepsilon_2 E_\rho^{cladding}(\rho = a), \tag{3.13f}$$

to obtain

$$\left[\frac{J_n'(u)}{u\,J_n(u)}+\frac{K_n'(w)}{w\,K_n(w)}\right]\left[\frac{\varepsilon_1}{\varepsilon_2}\frac{J_n'(u)}{u\,J_n(u)}+\frac{K_n'(w)}{w\,K_n(w)}\right]= \qquad (3.14)$$

$$n^2\left(\frac{1}{u^2}+\frac{1}{w^2}\right)\left(\frac{\varepsilon_1}{\varepsilon_2}\frac{1}{u^2}+\frac{1}{w^2}\right).$$

Combining Eqs. (3.12a) and (3.14), we can solve for u and w hence β_g.

3.3 LP_{01} and $LP_{11}{}^{even}$ modes

It is not a trivial matter to solve Eqs. (3.12a) and (3.14) for the latter equation is simply too complex to handle. To simplify Eq.(3.14), we assume

$$\Delta \ll 1. \qquad (3.15)$$

This equation implies the weakly-guiding or paraxial approximation and that the refractive index of core (n_1) is just slightly larger than that (n_2) of the cladding. Applying this weakly guiding condition, we can rewrite Eq.(3.14) as

$$\frac{u\,J_{m-1}(u)}{J_m(u)}=-\frac{w\,K_{m-1}(w)}{K_m(w)}, \qquad (3.16)$$

where

m = 1 corresponds to TM and TE modes,
m = n+1 corresponds to EH modes,
m = n -1 corresponds to HE modes,

$J_m(x)$ is the Bessel function of the first kind (order m), and $K_m(x)$ is the modified Bessel function of the second kind (order m). Eq.(3.16) is often referred to as the unified eigenvalue equation. Our goal is to combine Eqs. (3.12a) and (3.16) and solve for u and w. Using Eq.(3.11a) or (3.11b), the eigenvalue β_g (modal propagation constant) can be determined.

A particular eigenvalue β_g can be determined by the form of Eq.(3.16). It is possible that for several different values of m and n the eigenvalue equation (3.16) has the same form. The fact that different indices of m and n correspond to the same eigenvalue equation is referred to as mode degeneracy. D. Gloge [16] groups the degenerate modes and classifies all modes by virtue of eigenvalue equations. He refers to them as LP modes (Linearly Polarized Modes). For example, LP_{0L} (m=0) modes correspond to

$$\frac{u J_1(u)}{J_0(u)} = \frac{wK_1(w)}{K_0(w)}, \tag{3.17a}$$

which represents the HE_{1L} mode. And similarly LP_{1L} (m=1) modes correspond to

$$\frac{u J_1(u)}{J_0(u)} = - \frac{wK_1(w)}{K_0(w)}. \tag{3.17b}$$

This eigenvalue equation comprises TM_{0L}, TE_{0L} and HE_{2L} modes. The final solution of Eqs.(3.12a) and (3.16) is presented as Figure 3-1.

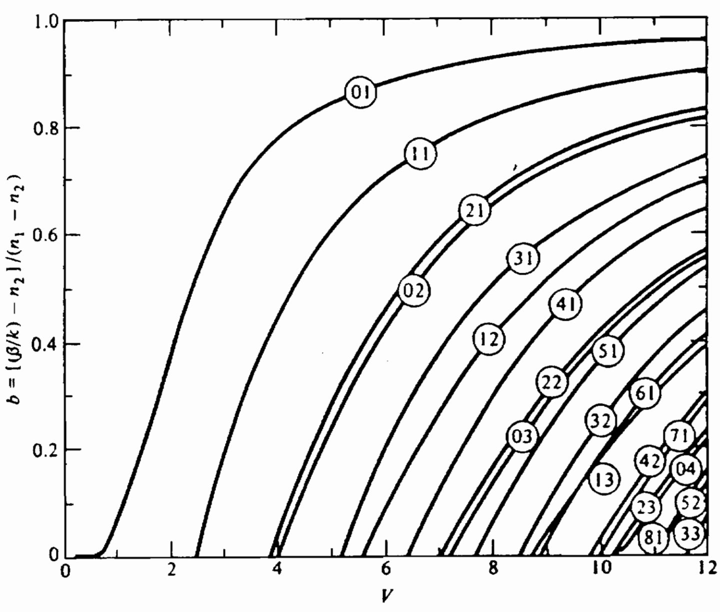

Figure 3-1. Plot of the propagation constant b as a function of V for various LP modes [17].

The vertical axis of the plot in Figure 3-1 is b, defined as

$$b = \frac{a^2 w^2}{V^2}, \tag{3.18a}$$

where

$$V = \frac{2\pi a}{\lambda}\left(n_1{}^2 - n_2{}^2\right)^{1/2}. \tag{3.18b}$$

For the weakly-guiding approximation,

$$b = \frac{\beta_g/k - n_2}{n_1 - n_2}, \tag{3.19}$$

where b is referred to as a normalized propagation constant. The horizontal axis is V. It has been shown [17] that the total number (M) of modes in the fiber can be approximated as

$$M = V^2/2. \tag{3.20}$$

Notice that V number is determined solely by the fiber structure and the light source.

The smallest eigenvalue β_g derived from the first root of Eq.(3.17a) is called the LP_{01} mode or fundamental mode. The next larger eigenvalue is obtained from the first root of Eq.(3.17b) and it is referred to as the LP_{11} mode. Studying Figure 3-1, we recognize that if V is set between 2.405 and 3.832, only the LP_{01} and LP_{11} modes can be excited. Under the weakly guiding condition, V is slightly larger than 2.405 since $\Delta << 1.0$. This is the two-mode operation that we want to achieve.

The LP_{11} mode contains TM_{01}, TE_{01} and HE_{21} modes for a circular wave guide. In an elliptical wave guide, this mode degeneracy is broken into two different modes, namely the $LP_{11}{}^{even}$ and $LP_{11}{}^{odd}$ modes [13]. To maintain the two-mode operation in an elliptical core fiber, we excite only the LP_{01} and $LP_{11}{}^{even}$ modes. Nevertheless, we still treat the wave guide as a circular core fiber in the future analysis.

3.4 Two-mode interference electric field expression

Having derived the algorithm for seeking wave propagation constants under the weakly-guiding condition and consulting Eq.(3.9), we can express the modal field amplitude of the linearly polarized LP_{lm} mode in the fiber core region as

$$\Psi_{lm} = A_{lm}\, J_l\, (\beta_{c,lm}\, \rho)\, \cos(l\phi)\, \exp(j\beta_{g,lm}\, z)\, \exp(-j\omega t), \qquad (3.21)$$

where $\beta_{c,lm}{}^2 = \omega^2 n_1{}^2 / c^2 - \beta_{g,lm}{}^2$, ω is the angular frequency of operation and $\beta_{g,lm}$ is the wave propagation constant of the mode. A_{lm} is the field amplitude coefficient of the mode, which depends upon the excitation condition. In the case of two-mode operation, since only the LP_{01} and $LP_{11}{}^{even}$ modes are excited in the waveguide, the electric field amplitudes can be expressed as

$$\Psi_{01} = A_{01}\, J_0\, (\beta_{c,01}\, \rho)\, \exp(j\beta_{g,01} z)\, \exp(-j\omega t), \text{ and} \qquad (3.22a)$$

$$\Psi_{11} = A_{11}\, J_1\, (\beta_{c,11}\, \rho)\, \cos(\phi)\, \exp(j\beta_{g,11}\, z)\, \exp(-j\omega t). \qquad (3.22b)$$

The total electric field at (ρ,ϕ,z) in the fiber core can be written as

$$\begin{aligned} \Psi &= \Psi_{01} + \Psi_{11} \\ &= A_{01}\, J_0\, (\beta_{c,01}\, \rho)\, \exp(j\beta_{g,01} z) + \\ &\quad A_{11}\, J_1\, (\beta_{c,11}\, \rho)\, \cos(\phi)\, \exp(j\beta_{g,11}\, z). \end{aligned} \qquad (3.23)$$

We ignore the $\exp(-j\,\omega\, t)$ factor in Eq.(3.23). The intensity at (ρ,ϕ,z) in the fiber core is

$$\begin{aligned} I &= \langle \Psi * \Psi^* \rangle \\ &= A_{01}{}^2\, J_0{}^2(\beta_{c,01}\, \rho) + A_{11}{}^2\, J_1{}^2(\beta_{c,11}\, \rho)\, \cos^2(\phi) + \\ &\quad 2\, A_{01}\, A_{11}\, J_0\, (\beta_{c,01}\, \rho)\, J_1(\beta_{c,11}\, \rho)\, \cos(\phi)\, \cos(\Delta\beta_g\, z), \end{aligned} \qquad (3.24)$$

where $\Delta\beta_g = \beta_{g,11} - \beta_{g,01}$ is the difference in the propagation constants between the LP_{01} and LP_{11}^{even} modes.

To discern the relationship between the spatial intensity distribution of the two-mode, e-core fiber and the external disturbances, i.e. strain and temperature, we examine Eq.(3.24) closely. We conclude that the first two terms represent a steady two-lobe pattern, which does not respond to external perturbations. It is the third term containing $\cos(\Delta\beta_g\, z)$ that is sensitive to perturbations due to strain and temperature. Let us define

$$\Delta\theta = \Delta\beta_g\, z, \tag{3.25}$$

as the differential phase delay between the LP_{01} and LP_{11}^{even} modes. The length of the fiber cavity, z, is a function of both strain (by fiber elongation) and temperature (by thermal expansion). To see the strain and temperature dependence of $\Delta\beta$, we go back to Figure 3-1 and Eqs.(3.18b) and (3.19). For a given V number between 2.405 and 3.832, there are two corresponding b's (b_{01} and b_{11}), and β_g 's ($\beta_{g,01}$ and $\beta_{g,11}$). Thus, we have, for the weakly-guiding approximation,

$$\Delta b\,(V) = \frac{\Delta\beta\,(V)}{k\,(n_1 - n_2)}, \text{ and} \tag{3.26}$$

$$\Delta\beta_g\,(V) = k\,(n_1 - n_2)\,\Delta b\,(V), \tag{3.27}$$

where $\Delta b = b_{01} - b_{11}$ and $\Delta\beta_g = \beta_{g,11} - \beta_{g,01}$. Since the V number is function of a, n_1 and n_2, which in turn are functions of both strain (ε) and temperature (T). Thus,

$$\Delta\beta_g = \Delta\beta_g\,(\varepsilon,T). \tag{3.28}$$

The variation of strain and temperature, hence $\Delta\theta$, will then cause an oscillation in the two-lobe spatial intensity pattern. Figure 3-2 shows the evaluation of this two-lobe pattern versus the differential phase delay $\Delta\theta$.

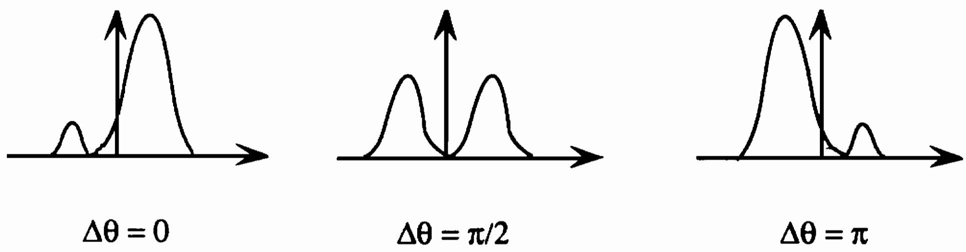

Figure 3-2. Two-lobe intensity patterns versus $\Delta\theta$ on the central axis of fiber core.

3.5 Output field expression of the two-mode and Fabry-Perot interferometers combined

Two partially reflective mirrors are incorporated into the two-mode, e-core fiber system as indicated in Figure 3-3, and the electric field at the fiber endface can be expressed as

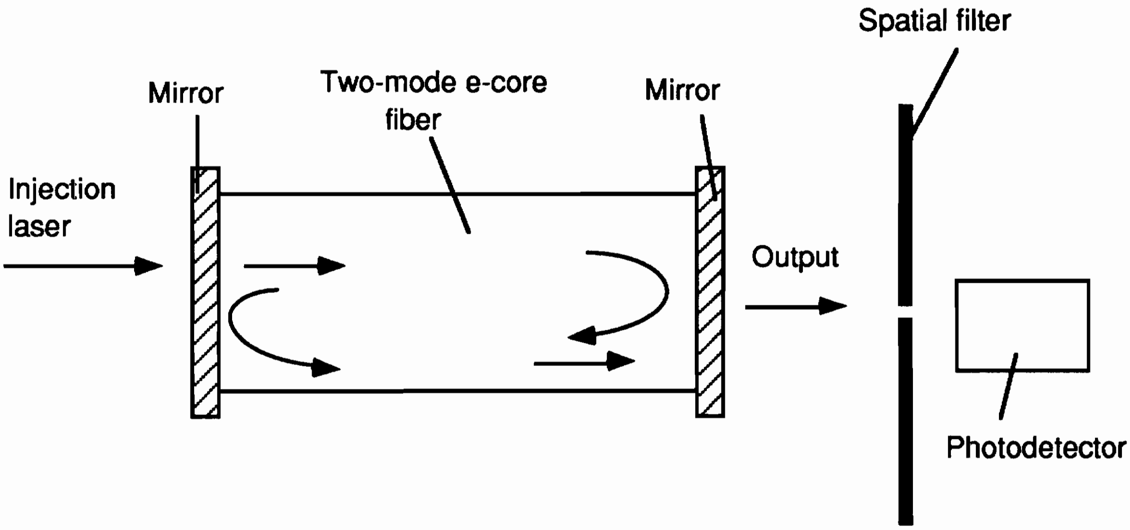

Figure 3-3. Two-mode, e-core IFPI etalon cavity.

For LP_{01}:

$$\Psi_{01} = A_{01} J_0 (\beta_{c,01} \rho) \exp(j\beta_{g,01}z) + A_{01} r_1 r_2 J_0 (\beta_{c,01} \rho) \exp(j\beta_{g,01}z) \exp(j2\beta_{g,01}z), \text{ and} \tag{3.29a}$$

for LP_{11}^{even}:

$$\Psi_{11} = A_{11} J_1 (\beta_{c,11} \rho) \cos(\phi) \exp(j\beta_{g,11}z) + A_{11} r_1 r_2 J_1 (\beta_{c,11} \rho) \cos(\phi) \exp(j\beta_{g,11}z) \exp(j2\beta_{g,11}z), \tag{3.29b}$$

where we ignore the exp(-jωt) factor. A_{01} and A_{11} are the excitation coefficients of the LP_{01} and LP_{11}^{even} modes, respectively. r_1 and r_2 are the reflective coefficients of mirror1 and mirror2, respectively. Here we consider only the primary transmissive and first two reflective waves at the output. The other multi-reflective waves are ignored for their field amplitudes are much smaller than those of the primary and first reflective waves. To simplify Eqs.(3.29a) and (3.29b), we assume that $r_1=r_2=r$ and $A_{01} = A_{11} = 1$ (equal excitation), to obtain

$$\Psi_{01} = J_0 (\beta_{c,01} \rho) \exp(j\beta_{g,01}z) (1 + r^2 \exp(j2\beta_{g,01}z)) = J_0 (\beta_{c,01} \rho) R_{01} \exp(j (\beta_{g,01}z + \alpha_{01})), \tag{3.30a}$$

and

$$\Psi_{11} = J_1 (\beta_{c,11} \rho) \cos(\phi) \exp(j\beta_{g,11}z) (1 + r^2 \exp(j2\beta_{g,11}z)) = J_1 (\beta_{c,11} \rho) \cos(\phi) R_{11} \exp(j (\beta_{g,11}z + \alpha_{11})), \tag{3.30b}$$

where

$$R_{01} = (1 + r^4 + 2 r^2 \cos(2\beta_{g,01}z))^{1/2}, \tag{3.31a}$$

$$\alpha_{01} = \arctan (r^2 \sin (2\beta_{g,01}z) / (1 + r^2 \cos (2\beta_{g,01}z))), \tag{3.31b}$$

and

$$R_{11} = (1 + r^4 + 2 r^2 \cos(2\beta_{g,11}z))^{1/2}, \tag{3.32a}$$

$$\alpha_{11} = \arctan (r^2 \sin (2\beta_{g,11}z) / (1 + r^2 \cos (2\beta_{g,11}z))). \tag{3.33b}$$

The total field amplitude at (ρ, ϕ, z) (fiber endface) is the

$$\Psi = \Psi_{01} + \Psi_{11}, \text{ and} \tag{3.33}$$

the total intensity can be written as

$$\begin{aligned} I &= \langle \Psi * \Psi^* \rangle \\ &= (J_0(\beta_{c,01}\rho) R_{01})^2 + (J_1(\beta_{c,11}\rho)\cos(\phi) R_{11})^2 + \\ &\quad + 2 J_0(\beta_{c,01}\rho) R_{01} J_1(\beta_{c,11}\rho) R_{11} \cos(\phi) * \cos(\Delta\beta_g z + \Delta\alpha), \end{aligned} \tag{3.34}$$

where $\Delta\alpha = \alpha_{11} - \alpha_{01}$. The results of a numerical computer calculation of the intensity from Eq.(3.34) versus fiber elongation is presented in Figure 3-4.

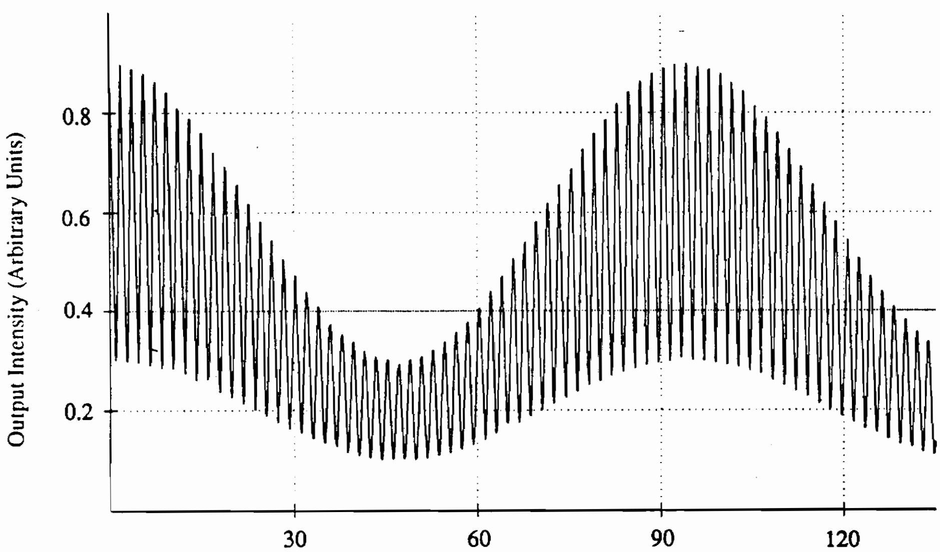

Figure 3-4. Sensor output versus fiber elongation in μm.

The long-period sine wave corresponds to the two-lobe oscillation and the high frequency sine wave corresponds to the intrinsic Fabry-Perot interference signal, which is modulated by the two-lobe interference signal. To further demonstrate the interference pattern, a twodimensional intensity distribution on the fiber cross section at the endface is calculated and mapped using Eq.(3.34). This pattern is shown in Figure 3-5 .

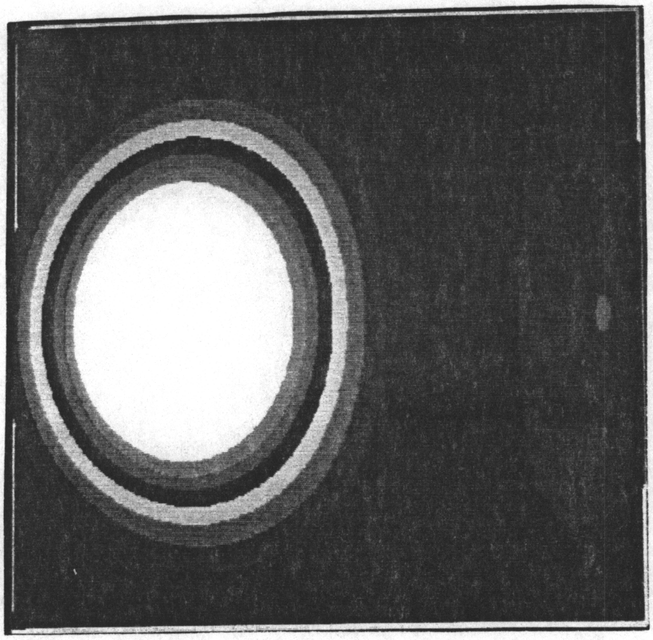

Figure 3-5. Spatial intensity distribution pattern over a cross section area of the fiber core ($\Delta\theta = \pi$).

The degrees of brightness represent different intensity values. The Fabry-Perot interference pattern cannot be seen here in this figure because the Fabry-Perot interference signal appears only when the length of fiber is changing.

4. Cross sensitivity

4.1 Definition of cross sensitivity

Cross sensitivity in the case of simultaneous measurement is the mutual dependence among the physical measurands. For the simultaneous measurement of strain and temperature, the optical signals due to strain and temperature are mixed in the measuring process. Therefore, two coupled equations must be solved simultaneously to separate the strain and temperature information.

4.2 Mathematical description of cross sensitivity (a first order approximation)

Studying Figures 2-3(a), 2-3(b) and 2-3(c), it is understood that Fabry-Perot ($\Delta\theta_1$) and the two-lobe ($\Delta\theta_2$) fringe signals must be counted to determine environmental effects. These interference phase signals are generated by several pairs of optical fields.

For the LP_{01} and LP_{11}^{even} modes interference, the optical path difference is

$$\theta_1 = \Delta\beta_g L, \tag{4.1a}$$

where $\Delta\beta_g = \beta_{g,01} - \beta_{g,11}$ and L is the length of the fiber. For Fabry-Perot interference, there are four major optical path differences. They are

$$\theta_2 = 2\beta_{g,01} L, \tag{4.1b}$$

$$\theta_3 = 2\beta_{g,11} L, \tag{4.1c}$$

$$\theta_4 = (2\beta_{g,01} - \beta_{g,11})L, \text{ and} \tag{4.1d}$$

$$\theta_5 = (2\beta_{g,11} - \beta_{g,01})L, \tag{4.1e}$$

where we consider only the first two reflected waves and ignore the other multi-reflected waves in the two-mirror cavity because their relative intensities are very small compared to those of the first two reflected waves. For the sake of discussion, Eqs. (4.1a) through (4.1e) can be unified as

$$\theta_j = \beta_j L, \tag{4.2}$$

where j = 1, 2 ,3, 4, 5 and

$\beta_1 = \Delta\beta_g$,

$\beta_2 = 2\ \beta_{g,01}$,

$\beta_3 = 2\ \beta_{g,11}$,

$\beta_4 = 2\ \beta_{g,01} - \beta_{g,11}$, and

$\beta_5 = 2\ \beta_{g,11} - \beta_{g,01}$.

In general, β_j and L are functions of both strain (ε) and temperature (T). Eq.(4.2) can be rewritten as

$$\theta_j(\varepsilon,T) = \beta_j(\varepsilon,T)\ L(\varepsilon,T). \tag{4.3}$$

In the vicinity of an initial state (ε_0,T_0), we use a Taylor expansion to obtain the expression when a strain ($\Delta\varepsilon$) and temperature change (ΔT) are applied simultaneously on the fiber, viz.,

$$\theta_j(\varepsilon,T) = \beta_j(\varepsilon_0,T_0)\ L(\varepsilon_0,T_0) + \left[\beta_j\frac{\partial L}{\partial \varepsilon} + \frac{\partial \beta_j}{\partial \varepsilon}L\right]^{T=T_0,\varepsilon=\varepsilon_0} \Delta\varepsilon$$

$$+ \left[\beta_j\frac{\partial L}{\partial T} + \frac{\partial \beta_j}{\partial T}L\right]^{T=T_0,\varepsilon=\varepsilon_0} \Delta T. \tag{4.4}$$

Eq.(4.4) then can be simplified to the form of the first order approximation.

$$\Delta\theta_j = \left[\beta_j\frac{\partial L}{\partial \varepsilon} + \frac{\partial \beta_j}{\partial \varepsilon}L\right]^{T=T_0,\varepsilon=\varepsilon_0} \Delta\varepsilon + \left[\beta_j\frac{\partial L}{\partial T} + \frac{\partial \beta_j}{\partial T}L\right]^{T=T_0,\varepsilon=\varepsilon_0} \Delta T\ . \tag{4.5}$$

The major reason for choosing the first order approximation is simplicity. The justification of this simplification is, as will be demonstrated in the next chapter, that the experimental data suggests that the number of fringes depends linearly on $\Delta\varepsilon$ and ΔT, respectively. It was also recognized experimentally that the four major Fabry-Perot interference signals (j= 2, 3, 4 and 5) could not be separated and they also largely depended upon the mode excitation condition. Hence, only the two-lobe interference and one Fabry-Perot interference (superposition of the four interferometers) fringe signals can be realistically recorded. Eqs.(4.1b) through (4.1e) are then regarded as one equation and, for j=1 and 2, Eq.(4.5) corresponds to Eqs.(2.2a) and (2.2b), respectively.

5 Experiments

5.1 Experiment guideline

Rewrite Eqs.(2.2a) and (2.2b) as

$$\Delta\theta_1 = A * \Delta\varepsilon + B * \Delta T, \text{ and} \tag{2.2a}$$

$$\Delta\theta_2 = C * \Delta\varepsilon + D * \Delta T, \tag{2.2b}$$

where $\Delta\theta_1$ and $\Delta\theta_2$ represent the phases induced by the Fabry-Perot and two-lobe interferometers, respectively. The strain and temperature dependence of $\Delta\theta_1$ and $\Delta\theta_2$ demonstrates the cross sensitivity effect. To resolve temperature and strain in the sensing system, these four coefficient constants A, B,C, and D must be determined. The rest of this chapter concerns four independent experiments for obtaining each of the four coefficients.

5.2 Fabry-Perot strain measurement

5.2.1 Experimental set-up

To obtain Fabry-Perot strain constant A in Eq.(2.2a), we strained the fiber while keeping the temperature constant ($\Delta T=0$). Eq.(2.2a) then becomes

$$\Delta\theta_1 = A * \Delta\varepsilon. \tag{5.1}$$

By counting the fringes induced by $\Delta\varepsilon$, the change of the Fabry-Perot phase $\Delta\theta_1$ and hence the constant A could be determined. The experimental set-up is shown in Figure 5-1.

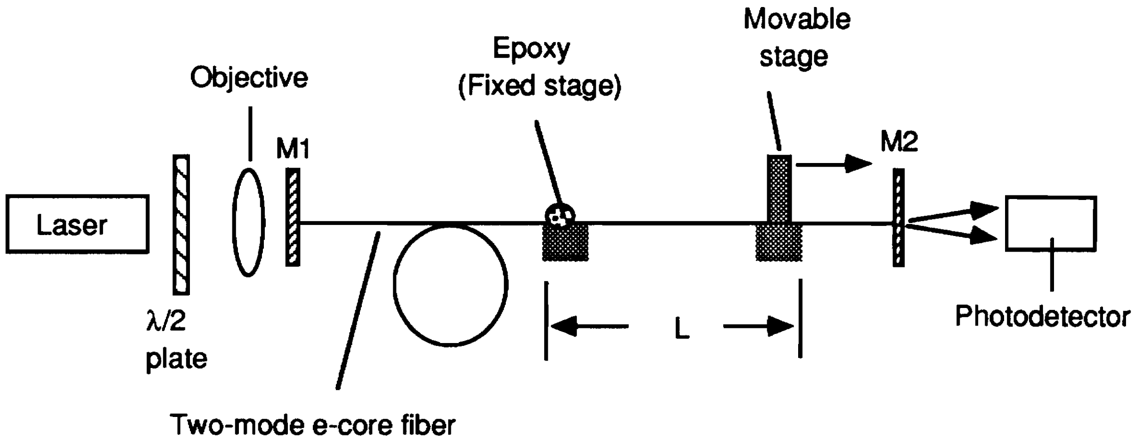

Figure 5-1. Fabry-Perot strain measurement experiment set-up (L= 57 cm).

5.2.2 Explanation of the experiment

The laser beam (λ= 633 nm) passing through a half wave plate ($\lambda/2$) was focused by a microscope objective into the two-mode, e-core fiber (manufactured by Andrew Corporation). The dimensions of the fiber core were 1.25 μm x 2.50 μm. The entire far field intensity pattern was collected by the photodetector. The laser light was linearly polarized with an unknown polarization direction. The function of the half wave plate ($\lambda/2$) was to rotate the polarization orientation of the laser light such that it aligned with either orthogonal polarization axis of the e-core fiber. This alignment guarantees a sharp and clean two-lobe far field intensity pattern [18] even though it was not important for this particular strain measurement. The other three experiments would use this half wave plate to obtain sharp and clean two-lobe intensity patterns in the far field. The section of two-mode, e-core fiber (L= 57 cm) was axially strained using a micropositioner (a movable stage). M1 and M2 are two partially reflective (31%) and transmissive (31%) mirrors, manufactured by Ealing Electro-Optics. A Fabry-Perot cavity was created by these two mirrors. The signal which appeared on the oscilloscope was due to the Fabry-Perot interference fringes caused by the straining effect.

5.2.3 Experimental result and discussion

A typical Fabry-Perot strain interference signal on oscilloscope is given in Figure 5-2.

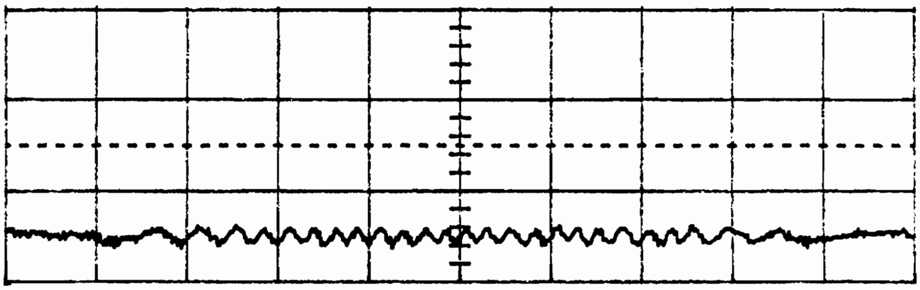

Figure 5-2. Fabry-Perot interference fringe signal for the strain of 6.6 μm elongation over a 57 cm long fiber. The scale of vertical axis is 500 mV per division and the scale of horizontal axis is 1 second per division.

Several such strain measurements were obtained and the results are tabulated in Table 5-1.

Table 5-1. Fabry-Perot strain measurement data (L= 57 cm)

Fiber elongation (μm)	Number of fringes	Phase induced (Rad/μm)
11.68	38	20.43
8.03	23	18.00
6.60	21	19.98
11.18	35	19.67
5.28	16	19.03
10.06	25	15.61

The average value of the Fabry-Perot strain coefficient over a 57 cm long fiber is

$$A = 19.42 \text{ rad}/\mu\text{m}. \tag{5.2}$$

It is worth mentioning that during the Fabry-Perot strain measurement, the fiber experienced a tension and was very sensitive to any external disturbance. The number of fringes was over counted, particularly at the starting and ending points of the straining process. It was estimated that two fringes were produced by manually adjusting the micropositioner at the starting and ending moments of the straining process, respectively.

5.3 Fabry-Perot temperature measurement

5.3.1 Experimental set-up

To determine the Fabry-Perot temperature coefficient B in Eq.(2.2a), we heated up or cooled down a small section of fiber and made sure that there was no strain on the fiber ($\Delta\varepsilon=0$). Thus Eq.(2.2a) is reduced to

$$\Delta\theta_1 = B * \Delta T. \tag{5.3}$$

By counting the fringes during the temperature change process, the phase change $\Delta\theta_1$ (due to ΔT) was obtained. Hence the constant B could be calculated using Eq.(5.3) . The experimental set-up is shown in Figure 5-3.

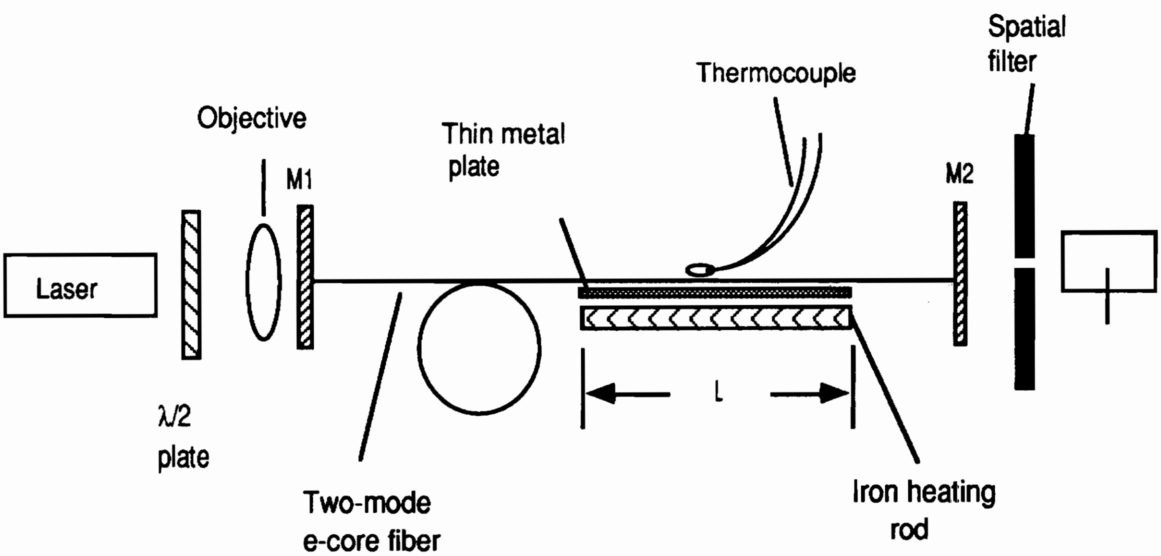

Figure 5-3. Fabry-Perot temperature measurement experimental set-up. M1 and M2 are two partially reflective and transmissive mirrors. The length (L) of the fiber under temperature exposure is 2.7 cm.

5.3.2 Explanation of the experiment

This experimental configuration here is similar to that of the case of the Fabry-Perot strain measurement in Figure 5-1. The major differences are that there is no straining device and there is a spatial filter (a 100 μm/ 130 μm multimode fiber) in front of the photodetector such that only a portion of the two-lobe intensity pattern could be collected. A section of the fiber (length L) was heated by an iron heating rod powered by an electrical current generator. A thin metal layer was put between the fiber and the heating rod to even out the temperature distribution on the fiber. A thermocouple head was placed very close to the fiber and thus it sensed the temperature the fiber experienced. During the temperature modulation process, the photodetector output gave both the two-mode interference signal and the interference signals produced by the light waves inside the two-mirror cavity.

5.3.3 Experimental result and discussion

A typical Fabry-Perot temperature interference signal oscilloscope trace is shown in Figure 5-4.

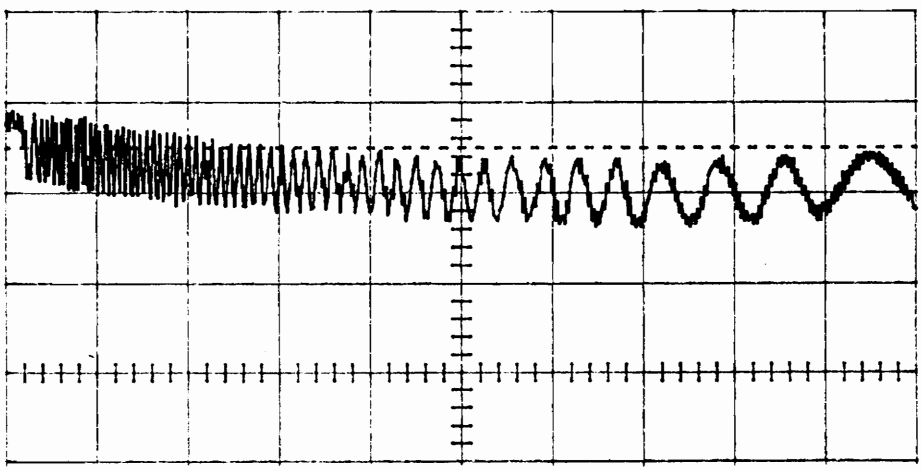

Figure 5-4. Fabry-Perot interference signal for temperature cooling from 76 °C down to 38 °C. The length of the fiber under temperature exposure is 2.7 cm. The vertical scale is 200 mV per division and the horizontal scale is 2 seconds per division.

Several such measurements were taken and the results are tabulated in Table 5-2.

Table 5-2. Fabry-Perot temperature data

Starting T (°C)	End T (°C)	Number of fringes	Phase induced (Rad./°C)
63	39	40.0	10.472
76	38	58.0	9.590

The average value of the Fabry-Perot temperature coefficient for an effective 2.7 cm long fiber is

$$B = 10.04 \text{ rad/°C}. \quad (5.4)$$

As mentioned earlier, in addition to Fabry-Perot temperature fringe signal in Figure 5-4 during the cooling process, the DC level of those fringe signals is decreased. This effect was caused by the two-lobe intensity pattern oscillation under the influence of temperature.

5.4 Two-mode strain measurement

5.4.1 Experimental set-up

Similarly, to find the two-mode strain coefficient constant C in Eq.(2.2b), we axially strained the fiber while keeping temperature constant ($\Delta T=0$). Eq.(2.2a) is reduced to

$$\Delta\theta_2 = C * \Delta\varepsilon. \quad (5.5)$$

Measuring the phase ($\Delta\theta_2$) induced by the strain $\Delta\varepsilon$, C could be calculated using Eq.(5.3) . The experimental set-up is shown in Figure 5-5.

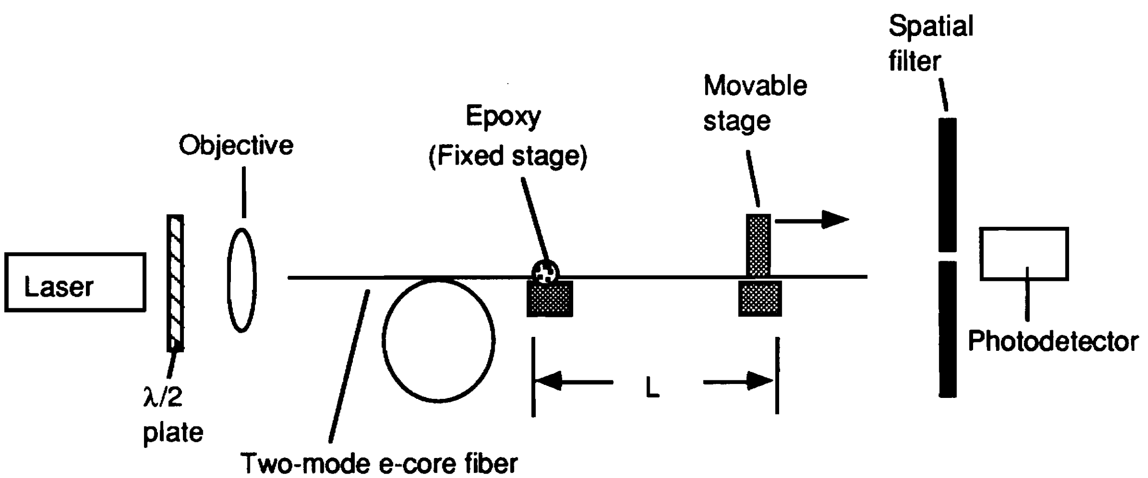

Figure 5-5. Two-mode strain measurement experimental set-up (L = 37.2 cm).

5.4.2 Explanation of the experiment

Since we were interested only in the two-mode interference signal, the two mirrors were removed. A section of fiber (length L = 37.2 cm) was fixed by two stages. One of the stages was permanently fixed and the other stage was movable. By controlling the movable stage, a precise axial strain could be applied on the fiber.

5.4.3 Experimental result and discussion

A typical two-mode strain interference signal oscilloscope trace is given in Figure 5-6.

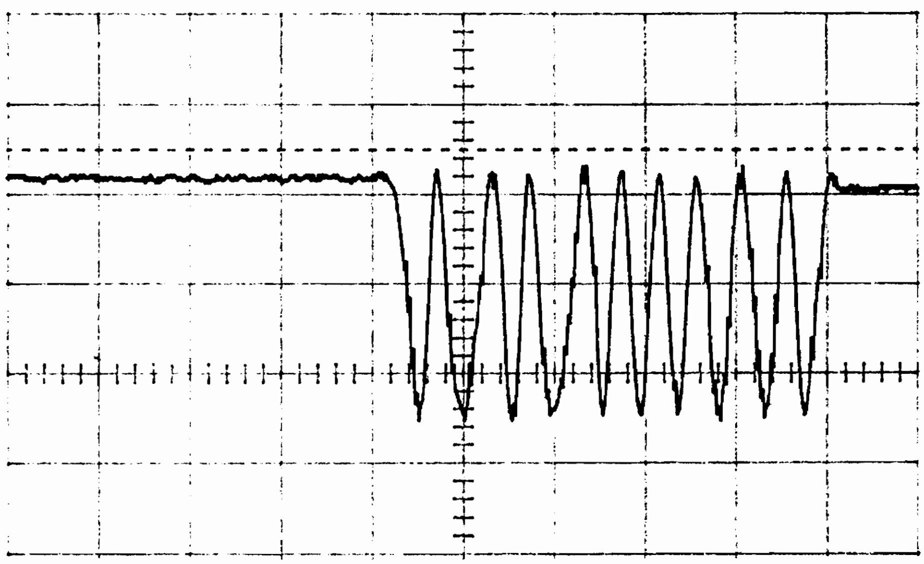

Figure 5-6. Two-mode interference signal for the strain of 800 μm elongation over a 37.2 cm fiber. The vertical scale is 1 V per division and the horizontal scale is 0.5 second per division.

Several such strain measurements were obtained and the results are tabulated in Table 5-3.

Table 5-3. Two-mode strain interference data (L = 37.2 cm)

Fiber elongation (μm)	Number of fringes	Phase induced (Rad./μm)
563.8	7.12	0.07939
800.1	10.00	0.07853
1028.7	13.00	0.07940
292.2	3.75	0.08066
254.0	3.12	0.07730

The average value of the two-mode strain coefficient over a 37.2 cm long fiber is

$$C = 0.079 \text{ rad}/\mu\text{m}. \tag{5.6}$$

5.5 Two-mode temperature measurement

5.5.1 Experimental set-up

To determine coefficient D in Eq.(2.2b), we heated up or cooled down a section of two-mode, e-core fiber under the condition of no strain ($\Delta\varepsilon$=0). Eq.(2.2a) is reduced to

$$\Delta\theta_2 = D * \Delta T. \tag{5.7}$$

By counting the fringes and recording ΔT, $\Delta\theta_2$, the phase induced, and hence the coefficient D could be found using Eq.(5.7).

The experimental set-up is shown in Figure 5-7.

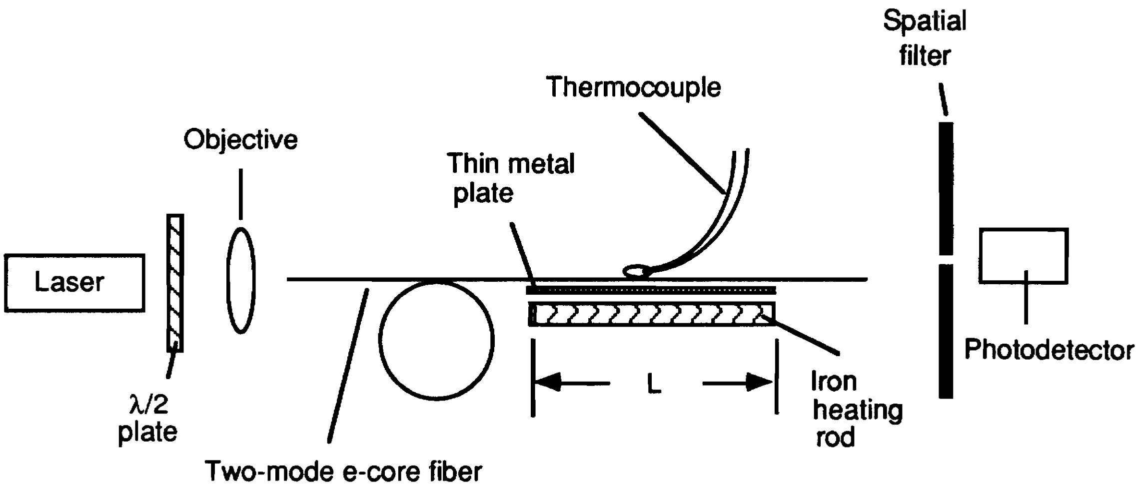

Figure 5-7.Two-mode temperature measurement set-up.

5.5.2 Explanation of the experiment

Instead of straining the fiber, a section of the fiber (length L) was heated by an iron heating rod similar to the case of Fabry-Perot temperature measurement in Figure 5-3. There was no axial strain on the fiber and no mirrors, therefore the reading at the photodetector represented the two-lobe interference signal induced solely by external temperature change.

5.5.3 Experimental result and discussion

Two typical two-lobe interference temperature signals on the oscilloscope induced by cooling and heating processes, respectively, are presented in Figure 5-8 (a) and (b).

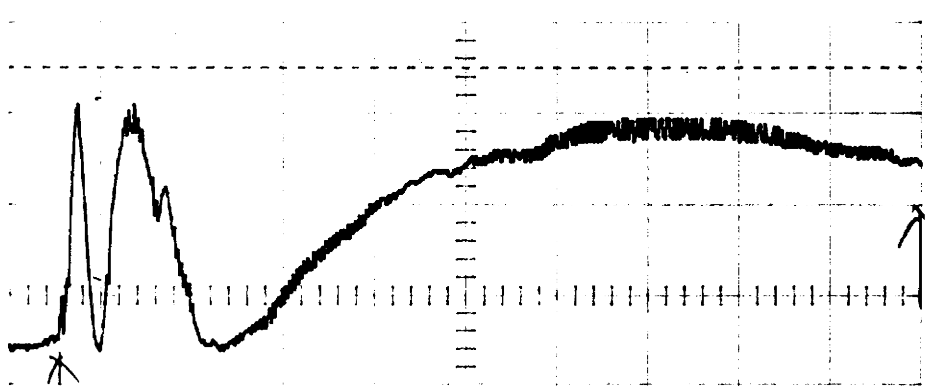

Figure 5-8 (a). Two-lobe interference signal for temperature cooling on a 16 cm long fiber from 297 °C down to 124 °C. The vertical scale is 1 V and the horizontal scale is 10 seconds.

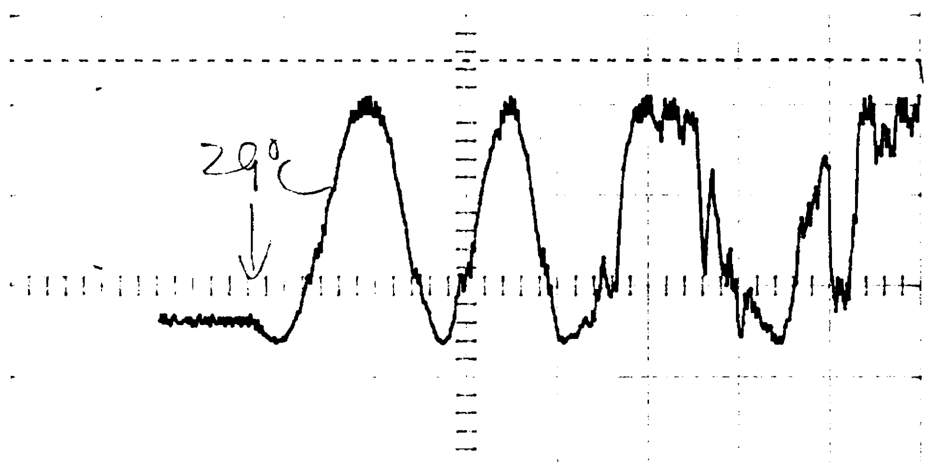

Figure 5-8 (b). Two-lobe interference signal for temperature increasing on a 16-cm-long fiber from 29 °C up to 279 °C. The vertical scale is 1 V per division and the horizontal scale is 100 seconds per division.

Many such temperature measurements were taken and the results are tabulated in Table 5-4.

Table 5-4. Two-lobe interference temperature data (L= 16 cm)

Starting T (°C)	End T (°C)	Number of Fringes	Phase induced (Rad./°C)
27	106	1	0.07953
106	176	1	0.08976
26	176	2	0.08378
176	205	0.5	0.10833
29	104	1	0.08378
104	170	1	0.09520
170	238	1	0.09240

The average value of the two-mode temperature coefficient (for L= 16 cm) is calculated to be

$$D = 0.087 \text{ rad/°C}. \tag{5.8}$$

To summarize the experimental results, we tabulate the determined four coefficients with their gauge lengths as

$$A = 19.42\ \mathrm{rad}/\mu\mathrm{m}, \qquad L = 57.0\ \mathrm{cm}.$$
$$B = 10.04\ \mathrm{rad}/^{\circ}\mathrm{C}, \qquad L = 2.7\ \mathrm{cm}.$$
$$C = 0.079\ \mathrm{rad}/\mu\mathrm{m}, \qquad L = 37.2\ \mathrm{cm}.$$
$$D = 0.087\ \mathrm{rad}/^{\circ}\mathrm{C}, \qquad L = 16.0\ \mathrm{cm}.$$

6. Resolution of the sensing system

6.1 Definition of resolution

Resolution of a fiber optic sensor is the minimum values of the measurands that the sensor can detect. Normally the direct outputs of fiber optic sensors are the encoding parameters, from which the measurands can be derived. In our case, the encoding parameters are the Fabry-Perot and two-mode interferometer phase changes ($\Delta\theta_1$ and $\Delta\theta_2$), and the measurands are strain ($\Delta\varepsilon$) and temperature (ΔT). To mathematically illustrate the concept of resolution, we define x and y as the two measurands and ξ_1 and ξ_2 as the two encoding parameters, respectively. The relationships among the encoding parameters and measurands can be expressed as

$$\xi_1 = f_1(x,y), \text{ and} \tag{5.1a}$$

$$\xi_2 = f_2(x,y), \tag{5.1b}$$

where f_1 and f_2 are analytic expressions. The differentiation of ξ_1 and ξ_2 with respect to x and y are given as

$$d\xi_1 = \frac{\partial f_1}{\partial x} dx + \frac{\partial f_1}{\partial y} dy, \text{ and} \tag{5.2a}$$

$$d\xi_2 = \frac{\partial f_2}{\partial x} dx + \frac{\partial f_2}{\partial y} dy. \tag{5.2b}$$

If $d\xi_1$ and $d\xi_2$ are the minimum detectable values of the encoding parameters, then dx and dy represent the resolutions of the measurands x and y, respectively. Using Eqs. (5.2a) and (5.2b), we can find the dx and dy as

$$dx = \left[\left(\frac{\partial f_2}{\partial y}\right) d\xi_1 - \left(\frac{\partial f_1}{\partial y}\right) d\xi_2\right]\left[\left(\frac{\partial f_1}{\partial x}\right)\left(\frac{\partial f_2}{\partial y}\right) - \left(\frac{\partial f_1}{\partial y}\right)\left(\frac{\partial f_2}{\partial x}\right)\right]^{-1}, \text{ and} \tag{5.3a}$$

$$dy = \left[\left(\frac{\partial f_2}{\partial x}\right) d\xi_1 - \left(\frac{\partial f_1}{\partial x}\right) d\xi_2\right]\left[\left(\frac{\partial f_1}{\partial y}\right)\left(\frac{\partial f_2}{\partial x}\right) - \left(\frac{\partial f_1}{\partial x}\right)\left(\frac{\partial f_2}{\partial y}\right)\right]^{-1}. \qquad (5.3b)$$

In our measurement of strain and temperature, both f_1 and f_2 are linear functions of x and y, as indicated in Eqs.(2.2a) and (2.2b). The four partial differentiation terms are the four coefficients.

6.2 Analysis of the resolution for the two-mode, e-core fiber sensor

Having determined A,B,C and D, we rewrite Eqs.(2.2a) and (2.2b) as

$$\Delta\theta_1 = (\ 19.42 \text{ rad/}\mu\text{m } \Delta\varepsilon \ + \ 3.719 \text{ rad/(cm °C) } \Delta T\ )\text{xL}, \qquad (5.4a)$$

$$\Delta\theta_2 = (\ 0.079 \text{ rad/}\mu\text{m } \Delta\varepsilon \ + \ 5.438\text{x}10^{-3} \text{ rad/(cm °C) } \Delta T)\text{xL}, \qquad (5.4b)$$

where the dimensions of ΔT and $\Delta\varepsilon$ are °C and μm/cm, respectively. $\Delta\theta_1$ and $\Delta\theta_2$ are expressed in radians. Here, L, the gauge length of the sensor, is introduced to balance the units of the simultaneous equations. Studying these coefficients carefully, we realized that the phase induced by Fabry-Perot interferometer is about several hundred times larger than the phase induced by the two-mode interferometer for a given external perturbation. Due to this large discrepancy, it is difficult to count these two fringe signals both accurately and simultaneously.

Numerically estimating the resolution of this sensing system, we consult Eqs.(5.3a) and (5.3b) and assume that the minimum phase changes (encoding parameters) that can be recognized in experiments are $500\text{x}2\pi/8$ and $2\pi/8$ (derived from the Fabry-Perot temperature measurement data) for the Fabry-Perot and two-lobe interferometers, respectively. We calculate that the minimum detectable temperature change and strain are 4.5 °C and 31μm/m (with a gauge length of 16 cm), respectively.

Another way to evaluate the quality of fiber optic simultaneous measurement systems is to study the coefficients of the simultaneous coupled equations. Vengsarkar *et al.* have presented a method of evaluating the resolution of a simultaneous measurement system [14]. Their method is to study the coefficients (A,B,C and D) and the relationship among them by calculating a condition number (rcond) of the coefficient matrix Λ, which is given as

$$\text{condition number} = \text{rcond}(\Lambda), \tag{5.5}$$

and

$$\Lambda = \begin{pmatrix} A & B \\ C & D \end{pmatrix}. \tag{5.6}$$

The criterion for comparison is: if Λ is well conditioned, the reciprocal of the condition number of the matrix, rcond(Λ), is near 1.0 and if Λ is ill-conditioned, rcond(Λ), is closer to zero. Reciprocals of condition numbers obtained in the past have been in the 0.01 - 0.1 range. The condition number of the coefficient matrix of Eqs.(5.4a) and (5.4b) is about 0.001, which is one order of magnitude less than most other simultaneous measurement schemes.

7.Conclusion

Optical fiber simultaneous measurement or multi-parameter measurement has gained a great amount of attention during the past several years. The research in this area is still in progress. The goal of simultaneous measurement has been to unambiguously determine physical measurands such as strain and temperature simultaneously utilizing less complicated systems. Such a measurement is of particular interest to smart structure applications. The objective of such research has been to explore and apply physical principles of optical fibers and to construct sensing systems for simultaneous measurement. Like the research areas of "absolute measurement" techniques and distributed sensors, simultaneous measurement is one of the most important research topics in the fiber optic sensor technology today.

Strain and temperature are the two most frequently encountered physical parameters in the environment of our interest. Generally, there are three steps to develop a sensing system to simultaneously resolve these two parameters employing a single piece of optical fiber. The first step is to identify two physical configurations pertaining to this fiber such that two different signals can be extracted. The second step is to employ these two output signals to mathematically set up two independent equations in which strain and temperature are considered as unknown variables. The final step is to devise a calibration procedure to experimentally determine all the coefficients in the two independent equations. The normal operation of the sensing system is to obtain the output signals experimentally and substitute these two pieces of information (encoding parameters) into the two coupled equations. Thereby, the strain and temperature can be determined by solving these two equations. The performance quality of the sensing system depends largely on the two physical configurations initially chosen.

Following this guideline, we have proposed a novel scheme of simultaneous measurement using two-mode, e-core fibers to measure both strain and temperature. The two physical configurations are the inherited two-mode interferometer within the fiber and an intrinsic Fabry-Perot interferometer, respectively. The Fabry-Perot interferometer is created by placing two partially reflective and transmissive mirrors on either end of this two-mode, e-core fiber. The output of these two interferometers are subject to changes under the variations of both strain and temperature. The output signal of this sensing system is therefore the Fabry-Perot interferometer fringe signal which is modulated by the two-mode interferometer fringe signal. Two types of phase information have been obtained experimentally. For the sake of simplicity, we set up two linear first order coupled equations, where strain and temperature are the two unknowns and there are four coefficients remained to be determined. Four independent experiments have been designed as a calibration procedure in which those four coefficients can be obtained. A resolution of 5 °C and 31µm/m for the gauge length of 16 cm has been achieved.

To evaluate the quality of this two-parameter sensing system, the cross sensitivity and resolution issues have been analyzed. Compared to many other fiber optic simultaneous measurement schemes, our sensor has a relatively low resolution and the quality of isolation between strain and temperature is below the average. The major reason for this is that there is an inherent mutual dependence between the two-mode and Fabry-Perot interferometers. In other words, these two physical configurations are not completely separated from one another. Despite these unfavorable factors, achievable advantages such as miniaturization, mass production (once the mirrors are deposited on the fiber endfaces) and the high sensitivity of the Fabry-Perot scheme lead us to believe that further research in the improvement of the resolution can lead to highly superior systems.

References

1. E. Udd, Fiber Optic Sensors (1990), Chapter 12. (John Wiley & Sons, Inc.)

2. E. Udd, Fiber Optic Sensors (1990), Chapter 3. (John Wiley & Sons, Inc.)

3. D. A. Jackson, R. Priest, A. Dandridge, and A. B. Tveten, Elimination of drift in a single-mode optical fiber interferometer using a piezoelectrically stretched coiled fiber, Appl. Opt. 19, 2926 (1980)

4. H. Hosokawa, J. Takagi, and T. Yamashita, Integrated optic microdisplacement sensor using a Y-junction and a polarization maintaining fiber, Optical Fiber Sensor Conference, Vol. 2 of OSA 1988 Technical Digest Series (Optical Society of America, Washington, D.C., 1988), pp. 137.

5. K. P. Koo, A.B. Tveten, and A. Dandridge, Passive stabilization scheme for fiber optic interferometers using (3x3) fiber directional couplers, Appl. Phys. Lett. 41, 616 (1982).

6. A. Olsson, C. L. Tang, and E. L. Green, Active stabilization of a Michelson interferometer by an electrooptically tuned laser, Appl. Opt. 19, 1897 (1980).

7. K. A. Murphy, W. V. Miller III, T. A. Tuan, A. M. Vengsarkar, and R. O. Claus, Miniaturized fiber-optic Michelson-type interferometric sensors, Appl. Opt., Vol .30, No.34, 5063 (1991).

8. B. Y. Kim, J. N. Blake, H. E. Engan, and H. J. Shaw, Opt. Lett. 11, 389 (1986).

9. J. N. Blake, B. Y. Kim, and H. J. Shaw, Opt. Lett. 11, 177 (1986)

10. A. Wang, K. A. Murphy, G. Z. Wang, A. M. Vengsarkar, and R. O. Claus, Micro-device for coupling, multiplexing, demultiplexing and switching using elliptical-core two-mode fiber, submitted to J. Lightwave Tech. (1992).

11. B.Y. Kim, J.N. Blake, S.Y. Huang, and H.J. Shaw, Use of highly elliptical core fibers for two-mode fiber devices, Opt. Lett. Vol.12, No. 9, 729 (1987).

12. A. Wang and G. Z. Wang, Analyses of near- and far- field two-lobe pattern outside the output endface of a two-mode fiber, submitted to J. Lightwave Tech., 1992

13. S. Y. Huang, J. N. Blake, and B. Y. Kim, Perturbation effects on mode propagation in highly elliptical core two-mode fibers, J. Lightwave Tech., Vol. 8, No. 1, 23 (1990).

14. A. M. Vengsarkar, W. G. Michie, L. Jankovic, B. Culshaw, and R. O. Claus, Fiber optic sensor for simultaneous measurement of strain and temperature, Proc. SPIE, Vol. 1367 , pp. 249260, (1990).

15. A. Wang, A. M. Vengsarkar, and R. O. Claus, Two-mode elliptical-core optical fiber sensors with temperature compensation, submitted to J. Lightwave Tech., 1991.

16. D. Gloge, Weakly guiding fibers, Appl. Opt., Vol. 10, No. 10, 2252 (1971).

17. G. Keiser, Optical Fiber Communications (2nd edition), pp. 44-47. (McGraw-Hill, Inc.)

18. A. M. Vengsarkar, B. R. Fogg, K. A. Murphy, and R. O. Claus, Polarimetric analysis of two-mode, elliptical-core optical fibers, Opt. Lett., Vol. 16, No. 7, 464 (1991).

Vita

Zhi G.Wang was born on February 5, 1963 in Wuhan, China. He had his primary, middle school and most of the high school education in Hubei province of China. In 1979 he moved with his family to Guangzhou, China. The following year he entered Zhongshan University studying computer science and received an associate degree in Spring 1982. After working as a computer programmer for two years in the Microelectronics Research Institute of the same university, he went to Southern University in Baton Rouge, Louisiana, to study physics in Spring 1985, and obtained his B.S. degree in Spring 1988. In the fall of the same year, he entered Washington University in St. Louis, Missouri, as a graduate student in physics and obtained his M.A. degree in Fall 1989. The following spring he came to Virginia Tech as a graduate student in electrical engineering, concentrated on fiber optics technology and expects to defend his masters degree thesis in June 1992.